

## Research



**Cite this article:** Gau J, Gravish N, Sponberg S. 2019 Indirect actuation reduces flight power requirements in *Manduca sexta* via elastic energy exchange. *J. R. Soc. Interface* **16**: 20190543.  
<http://dx.doi.org/10.1098/rsif.2019.0543>

Received: 2 August 2019

Accepted: 20 November 2019

**Subject Category:**

Life Sciences—Physics interface

**Subject Areas:**

biomechanics, biomaterials

**Keywords:**

flight, exoskeleton, *Manduca*, flapping, indirect actuation

**Author for correspondence:**

Jeff Gau

e-mail: [jeff.gau@gatech.edu](mailto:jeff.gau@gatech.edu)

Electronic supplementary material is available online at <https://doi.org/10.6084/m9.figshare.c.4764590>.

# Indirect actuation reduces flight power requirements in *Manduca sexta* via elastic energy exchange

Jeff Gau<sup>1,2</sup>, Nick Gravish<sup>5</sup> and Simon Sponberg<sup>1,3,4</sup>

<sup>1</sup>Interdisciplinary Bioengineering Graduate Program, Georgia Institute of Technology, Atlanta, GA 30332, USA

<sup>2</sup>George W. Woodruff School of Mechanical Engineering, Georgia Institute of Technology, Atlanta, GA 30332, USA

<sup>3</sup>School of Physics, and <sup>4</sup>School of Biological Sciences, Georgia Institute of Technology, Atlanta, GA 30332, USA

<sup>5</sup>Mechanical and Aerospace Engineering, University of California San Diego, San Diego, CA 92161, USA

JG, 0000-0003-1367-3848; NG, 0000-0002-9391-2476; SS, 0000-0003-4942-4894

In many insects, wing movements are generated indirectly via exoskeletal deformations. Measurements of inertial and aerodynamic power suggest that elastic recovery of energy between wingstrokes might reduce power requirements of flight. We tested three questions. (1) Can the thorax itself provide significant energy return? (2) Does a simple damped elastic model describe the bulk mechanical behaviour? (3) Are different regions of the thorax specialized for elastic energy exchange? We measured deformation mechanics of the hawkmoth *Manduca sexta* thorax by recording the force required to sinusoidally deform the thorax over a wide frequency range. Elastic energy storage in the thorax is sufficient to minimize power requirements. However, we find that a structural (frequency-independent) damping model, not a viscoelastic model, best describes the thorax's mechanical properties. We next performed complementary experiments on a structurally damped homogeneous hemisphere. In contrast to the hemispherical shell, we find that mechanical coupling between different regions of the thorax improves energy exchange performance and that local mechanical properties depend on global strain patterns. Specifically, the scutum region provides energy recovery with low dissipation, while the majority of energy loss occurred in the wing hinge region, highlighting the specificity of thorax regions for flight energetics.

## 1. Introduction

Indirect actuation is a prevalent feature among flying insects. Unlike traditional skeletal muscle attachments, the power muscles in many insects indirectly generate wing movements by deforming a continuous exoskeleton surrounding the thorax [1]. Like the complex interactions between power limited muscles, non-ideal latches and imperfect springs in power amplified biological systems [2], the introduction of the deformable exoskeleton could have significant consequences on flight mechanics. The thorax is a materially heterogeneous structure with complex geometry that contributes to coupled motion of wings and, in dipterans, halteres [3]. The thorax's frequency response may cause some wingbeat frequencies to be energetically favourable, thereby encouraging flight within a narrow band as seen in *Manduca sexta* [4] and *Apis mellifera* [5]. In addition, for the past 60 years, it has been thought that these exoskeletal deformations may reduce the energy required for flight by providing elastic energy storage and return. However, it remains unclear what the thorax's overall capacity for elastic energy return is, the extent of damping, and what factors give rise to its spring-like properties. To examine this role of thorax elasticity, we first explore the mechanical properties of the isolated thorax. We then compare these to simple mathematical and physical models of damped elastic structures, and finally, we examine how regional heterogeneity in the thorax contributes to its overall spring-like properties.

The mechanical power required for flapping-wing motion can be roughly divided into two components: inertial power ( $P_{\text{inertial}}$ ) required to accelerate and

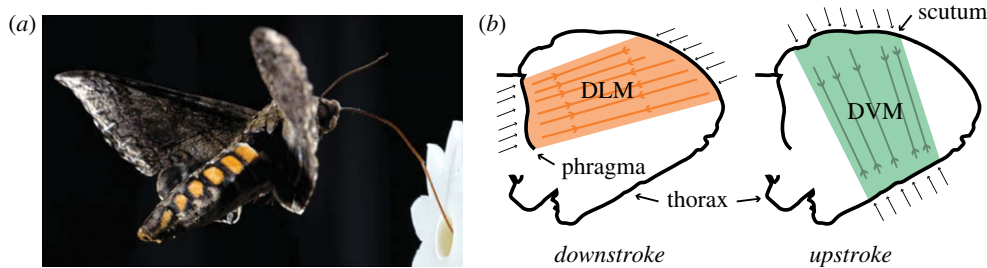


**Figure 1.** Insects with indirect actuation deform their exoskeleton to move their wings. (a) The hawkmoth *Manduca sexta* uses indirect actuation to fly. (b) Two sets of muscles, the dorsolongitudinal (DLM) and dorsoventral (DVM) attach to the thorax. The DLM attaches to the posterior phragma, which is an insertion of the exoskeleton into the thorax. The DVM attaches to the scutum, a smooth plate on the top of the thorax. The DLM and DVM act against each other to drive the upstroke and downstroke movements by deforming the thorax. (Online version in colour.)

decelerate the wings and aerodynamic power ( $P_{\text{aero}}$ ) required to overcome drag and generate lift. If we make the following basic assumptions: (1) symmetric upstroke and downstroke wing motion, (2) no energetic costs of wing deceleration, (3)  $P_{\text{aero}} < P_{\text{inertial}}$  and (4) zero elastic energy exchange, then the total power required for flight is  $P_{\text{total}} = (P_{\text{aero}} + P_{\text{inertial}})/2$  [6,7]. Under these conditions, the insect must only provide mechanical power during the acceleration phase of each half stroke because  $P_{\text{inertial}}$  is converted into  $P_{\text{aero}}$  during deceleration. However, if we assume there are spring-like structures in the insect flight system, excess wing kinetic energy can be absorbed and returned by elastic elements ( $P_{\text{return}}$ ). In an ideal case,  $P_{\text{total}} = P_{\text{aero}}$ . Because  $P_{\text{aero}} < P_{\text{inertial}}$ , this corresponds to a net reduction in  $P_{\text{total}}$ . Under this condition, all excess inertial power ( $P_{\text{inertial}} - P_{\text{aero}}$ ) is stored in spring-like structures and returned to reduce  $P_{\text{inertial}}$  for the subsequent half stroke [6,7].

Previous modelling and experimental efforts all point to elastic energy storage in the thorax and muscles as a mechanism for power reduction. However, these approaches all estimate elasticity through indirect measurements such as fluid dynamics or respirometry [7–11]. Blade element models, computational fluid dynamics and tomographic particle image velocimetry estimates suggest that perfect elastic energy exchange could reduce  $P_{\text{total}}$  by up to 20–35% in *Manduca sexta* [9–11]. These estimates indicate the potential benefits of elastic energy storage in flapping wing systems. However, there is a lack of direct mechanical measurements of the insect thorax to determine if elastic energy storage and recovery occurs under flight conditions.

There are several potential sources of elastic energy exchange in insect flight. The antagonistic extension of elastic elements in both passive and active muscle as well as exoskeletal deformations may store and return elastic energy (figure 1b) [12–15]. In particular, temperature gradients in *Manduca sexta* enable crossbridges within the flight power muscles to remain bound and function as springs, although the energy exchange capacity has not been quantified [15]. Unlike muscle, it is unclear what factors would enable substantial elastic energy exchange in the exoskeleton. While the exoskeleton is composed of resilient materials, such as resilin and chitin, material properties are not the sole determinant of bulk mechanical properties [16–18]. For instance, mechanical coupling of bending and stretching due to a structure's shape can significantly alter bulk mechanics [19]. In addition, large amplitude heterogeneous strain may concentrate deformations in regions with unfavourable properties for energy exchange (figure 2d) [21]. Thus, interactions between exoskeletal shape and material composition are significant for determining elastic energy

exchange capacity. While active muscle, passive muscle and the exoskeleton may all return elastic energy, there is a maximum useful elastic energy return beyond which  $P_{\text{total}}$  is not affected.

In addition to energy recovery, energy loss during thorax deformations ( $P_{\text{lost}}$ ) may substantially alter flight power requirements. Biological springs can introduce substantial frequency-dependent damping [18,22]. Similar to  $P_{\text{aero}}$ , any dissipation in the thorax is unrecoverable. If  $P_{\text{lost}}$  exceeds  $P_{\text{return}}$ , then the net effect of thorax deformations actually increases  $P_{\text{total}}$ . Furthermore, if damping is frequency dependent as seen in passive and active flight muscle [22], then there may be energetically preferable wingbeat frequencies and possible limits on the range of energetically attainable wingbeat frequencies.

We hypothesize that the thorax acts as a damped spring that substantially reduces  $P_{\text{total}}$ . To test this hypothesis, we employed a custom vibration apparatus to measure the thorax's passive mechanical properties under physiological conditions. We provided an oscillatory displacement to the thorax, mimicking the action of the flight power muscles. We measured the force required to deform the thorax to determine elastic energy storage and recovery in a typical wingbeat. We then analysed frequency sweep data to develop a mathematical model of thorax deformation mechanics. Despite obtaining this model, it was unclear what factors determine spring and damper-like properties in the thorax. To assess whether the passive musculature or exoskeletal shell dictate thorax mechanics, we repeated experiments with removed musculature. Finally, to quantify the role of different thorax regions on flight energetics, we performed complementary experiments on a homogeneous hemispherical shell (ping pong ball).

## 2. Methods

### 2.1. Animals

*Manduca sexta* used in these experiments were obtained as pupae from colonies maintained at the University of Washington and Case Western Reserve University. Moths were kept on a 12 L : 12 D cycle. We used seven males and 27 females between 1 and 7 days post-eclosion. Moth mass equalled  $2.13 \pm 0.47$  g.

### 2.2. Thorax preparation

Following a 30 min cold anaesthesia, we removed the head, abdomen, wings and legs from each moth to isolate the thorax. In some preparations ( $N = 10$ ), we removed the flight musculature, while in others we left the muscle intact ( $N = 24$ ). For the intact muscle

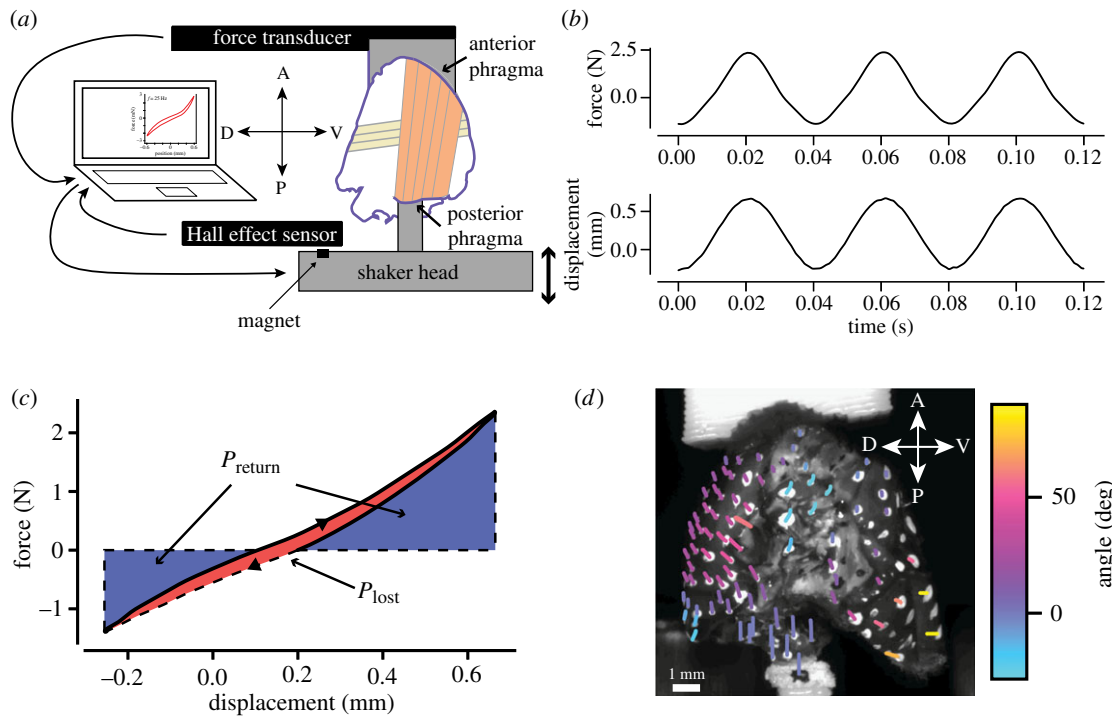


**Figure 2.** Experimental overview. (a) Experimental set-up. The second and third thoracic segments are mounted between a dynamic mechanical testing device and a force transducer. We prescribe a sinusoidal length input to physiological amplitudes and measure the force required to deform the thorax. (b) Representative force and displacement measurements from an intact thorax with passive musculature at 25 Hz. (c) Force–displacement plot from the same data as (b), but averaged over all oscillations. Blue area denotes  $P_{\text{return}}$  while red area denotes  $P_{\text{lost}}$ . The displacements are asymmetric because the operating length of downstroke muscles is 0.21 mm shorter than rest length [20]. (d) Visualization of strain through the second thoracic segment during a physiological oscillation at 1 Hz. We recorded high-speed video at 200 fps. White and black dots were painted on the thorax to aid in tracking. Colour denotes deformation angle off of the vertical while traces highlight the movement of each tracked point. (Online version in colour.)

preparations, we silenced neural activity by cutting the outward projections of the thoracic ganglion to the flight musculature. We then removed the first thoracic section to provide access to the anterior phragma for mounting on the shaker apparatus (figure 2a). Removing the first thoracic segment should not alter the mechanical properties of the flight apparatus because the first segment is small, attached to the second segment with soft tissue, and only the second and third segments are involved in flight [23]. Finally, we used damp wipes and compressed air to remove scales from the exoskeleton.

### 2.2.1. Muscle removal

The anterior and posterior ends of the pterothorax have large openings to remove muscle. We used forceps and scalpels to remove flight muscle from the pterothorax. We ensured that we removed at least 0.1 g of muscle, which is in rough agreement with previous reports of DLM muscle mass [24]. Any remaining pieces of muscle were negligible because we ensured that they only had one intact attachment point. Therefore, these muscle remnants could not be stretched and generate significant force during our experiments.

## 2.3. Thorax manipulations

### 2.3.1. Wing joint and scutum isolation cuts

These cuts removed material in the exoskeleton to isolate strain to certain functional regions (figure 3a,b). For the isolated joint condition, we removed the scutum to isolate strain to the wing joint. For the isolated scutum condition, we removed the wing joint to isolate strain to the scutum. The total material displaced in the isolated joint plus isolated scutum conditions should equal that of an intact thorax because the dorsal regions of the thorax are largely decoupled from the ventral.

### 2.3.2. Strain disruption cuts

For these manipulations, we used a series of cuts to disrupt strain through the exoskeleton without removing material (figure 3d,e). The objective of these cuts was to disrupt the transverse arch, which is known to increase longitudinal stiffness. For the longitudinal cut condition, we used a razor blade to cut a single anterior–posterior cut along the midline of the scutum. We then performed the triple longitudinal cut condition in which two parallel cuts are made on either side of the first longitudinal cut. This created three anterior–posterior cuts on the scutum.

## 2.4. Shaker preparation

We used cyanoacrylate glue to secure a three-dimensional printed shaft to the posterior phragma (figures 1b and 2a,d). This shaft was then mounted to the head of a custom shaker mechanism as described in [25]. On the anterior end, we used cyanoacrylate to rigidly attach the anterior phragma to a cantilever beam force transducer rated to 10 N with a resonance frequency of 300 Hz (FORT1000, World Precision Instruments, Sarasota, FL). The force transducer itself was mounted to a three-axis micromanipulator, which enabled us to precisely set the rest length of the thorax. Using the force transducer, we weighed the ABS attachment pieces plus cyanoacrylate. After mounting the thorax vertically, we returned the force to match this weight. We then adjusted the micromanipulator to precompress the thorax with an offset of 0.21 mm, which is the *in vivo* offset observed in *Manduca sexta* DLM during tethered flight [20]. To measure thorax compression and tension, we used an analogue hall effect sensor (DVR5053-Q1, Texas Instruments, Dallas, TX). This sensor was calibrated to measure the position of a permanent magnet attached to the shaker head. We drove the shaker head with an electrodynamic vibration testing system (VTS 600, Vibration Test Systems, Aurora, OH). Critically, the anterior and posterior phragmas are

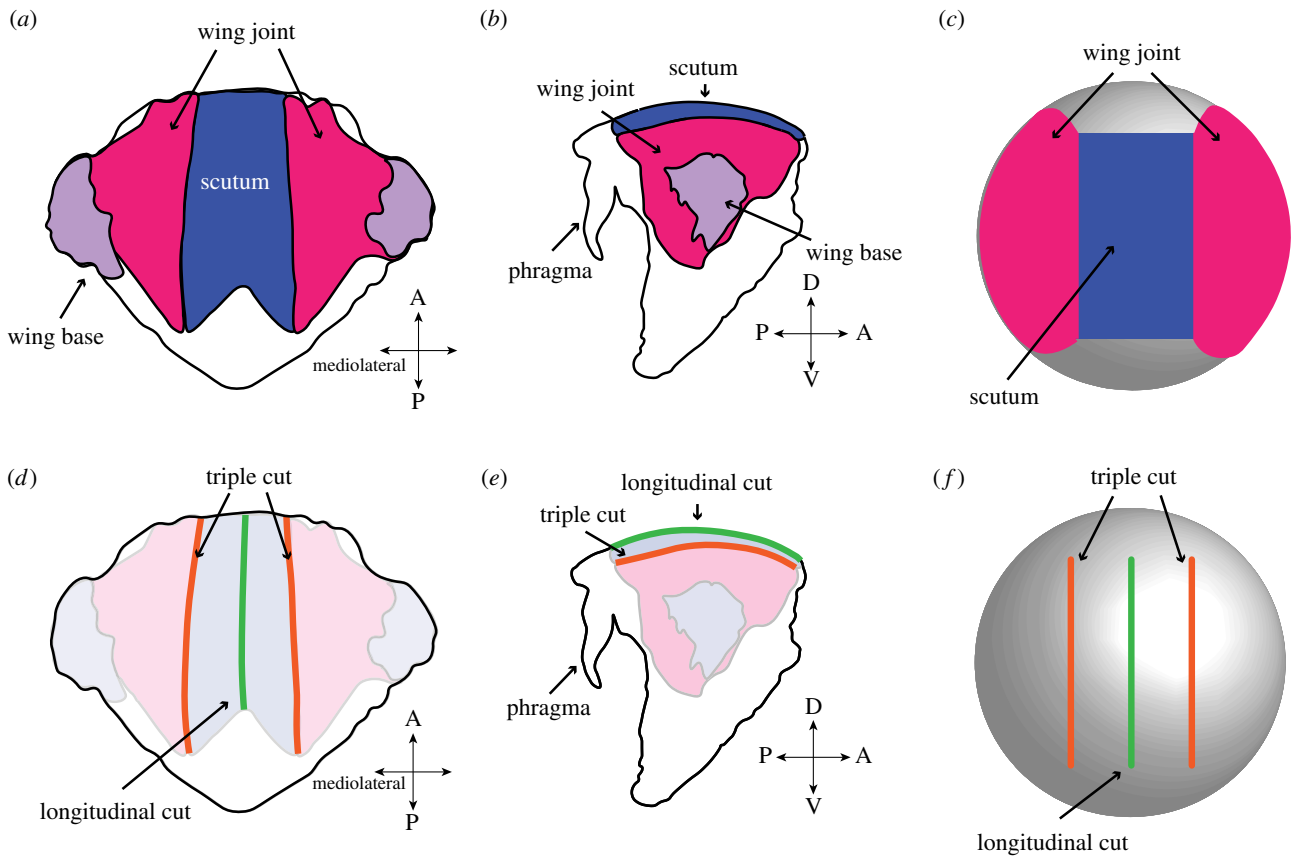


**Figure 3.** Thorax manipulations. (a–c) Region isolation experiments. (a) Dorsal view of the second thoracic segment, which contains the majority of flight muscle and forewings. The wing joint is in pink, scutum in blue and wing base in purple. (b) Lateral view of the second thoracic segment. In addition to the regions labelled in (a), the phragma is visible. (c) Analogous dorsal view of a ping pong ball highlighting the regions labelled in (a). (d–f) Strain disruption experiments. Dorsal (d) and lateral (e) views of the second thoracic segment. In addition to the features described above, the green line marks the longitudinal cut condition, while orange lines mark the triple cut. (f) Analogous dorsal view of a ping pong ball highlighting the cuts labelled in (d). (Online version in colour.)

the structures to which the downstroke power muscles attach *in vivo*. Attaching our experimental apparatus to these structures and displacing along the contraction axis of the main downstroke muscle (DLM) axis ensured physiologically relevant deformations.

## 2.5. Dynamic mechanical testing

After precompressing the thorax, we prescribed sinusoidal displacements to a physiological amplitude of 0.46 mm over a frequency sweep from 0.1 to 90 Hz. This frequency range encompasses the hawkmoth's wingbeat frequency of 25 Hz and the displacement amplitude corresponds to the *in vivo* DLM strain amplitude of 4.5% observed previously in *Manduca sexta* [20]. We acknowledge that individual thoraxes undergo different strain amplitudes, but the anatomy of *Manduca sexta* prevented us from measuring *in vivo* strain measurements without irreversibly damaging the thorax. This method of using mean strains from other individuals is well established in the literature [20,24]. After each experiment, we measured thorax/DLM length, which we defined as the distance between anterior and posterior phragma (figure 2a). We found that we had prescribed a strain of  $4.5 \pm 0.2\%$ . For a few thoraxes, we determined the number of oscillations needed to reach steady periodic oscillations, which we visually identified as no change in baseline drift. For all analyses in this paper, we only analysed oscillations after reaching this state.

## 2.6. Strain mapping

In one thorax, we mapped two-dimensional strain in the parasagittal plane. We removed the third thoracic segment to visualize the phragma and left the flight muscle intact. We then painted small white and black dots on the thorax to aid

strain visualization (figure 2d). We deformed the thorax at 1 Hz while recording from a machine vision camera at 200 Hz (electronic supplementary material, video S1; BlackFly S BFS-U3-4S2M-CS, FLIR Integrated Imaging Solutions, Inc. Richmond, BC, Canada).

## 2.7. Ping pong ball preparation

We repeated the analogous procedures to prepare ping pong balls. We chose ping pong balls because they are highly uniform, precisely spherical, and made of a material, celluloid, known to have structurally damped properties [26]. Because ping pong balls are spherical and homogeneous, there is no true 'scutum' or 'wing hinge'. We therefore visually determined analogous 'scutum' and 'wing hinge' regions. Similar to the thorax, we used ABS shafts to attach the ping pong ball to the custom shaker. For dynamic material testing, we used a displacement of 0.5 mm and precompression of 0.2 mm. We found that ping pong balls had similar peak forces to the thoraxes, indicating the thorax and ping pong ball experiments were in similar dynamic regimes for the shaker apparatus.

## 2.8. Desiccation control

To assess the effects of desiccation on thorax properties, we report  $P_{\text{return}}$  and  $P_{\text{lost}}$  on three thoraxes with passive musculature (electronic supplementary material, figure S1). Following the dynamic mechanical testing procedure outlined above, we repeatedly measured  $P_{\text{return}}$  and  $P_{\text{lost}}$  to assess the effects of desiccation on elastic energy exchange. We found that both  $P_{\text{return}}$  and  $P_{\text{lost}}$  increased with time, but that the conclusions in this report hold true regardless of desiccation effects.

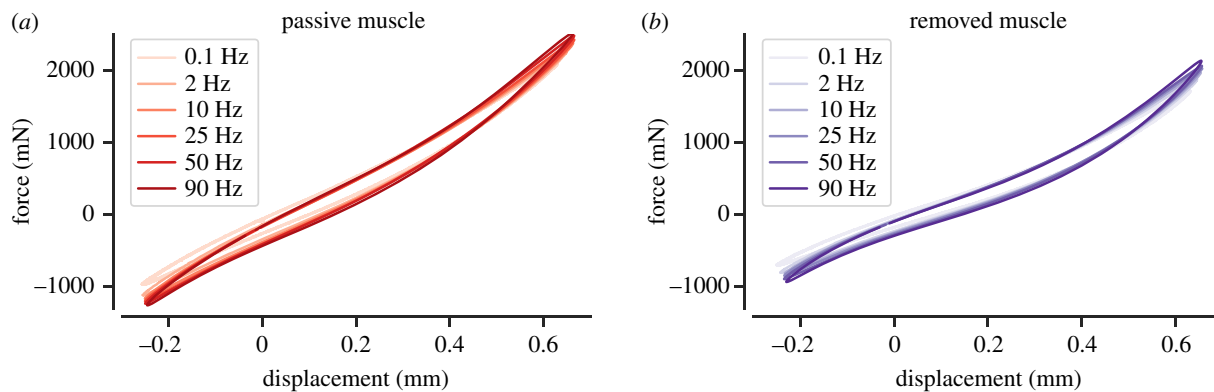


**Figure 4.** Force–displacement traces at representative frequencies from 0.1 to 90 Hz for an intact thorax with (a) passive muscle ( $N = 24$ ) and (b) removed muscle ( $N = 10$ ). For each frequency, the traces represent the average force and average displacement at each time point. Positive displacement denotes compression. (Online version in colour.)

## 2.9. Reverse frequency sweep control

To ensure that sweep direction did not influence our conclusions, we performed frequency sweeps from 0.1 to 90 Hz on four thoraxes followed immediately by a sweep from 90 to 0.1 Hz. We found no noticeable differences between sweep directions (electronic supplementary material, figure S2).

## 2.10. Data analysis

### 2.10.1. Empirical calculations of power exchange

We calculated three body mass-specific powers: power required to drive the displacements ( $P_{\text{in}}^*$ ), power returned via elastic energy storage and return ( $P_{\text{return}}^*$ ) and power dissipated during an oscillation ( $P_{\text{lost}}^*$ ).  $P_{\text{in}}^*$  is the sum of  $P_{\text{return}}^*$  and  $P_{\text{lost}}^*$ . Because the wings have been removed,  $P_{\text{in}}^*$  is just the power necessary to deform the thorax and accelerate thoracic mass. We begin by empirically integrating force over displacement to determine the analogous energy metrics (figure 2c). We multiply energy by oscillation frequency to arrive at power. We then normalize by body mass to arrive at body mass-specific powers ( $P^*$ ). Finally, we calculate resilience ( $R$ ), which is a measure of spring efficiency, as

$$R = \frac{P_{\text{return}}^*}{P_{\text{in}}^*}. \quad (2.1)$$

### 2.10.2. Thorax elastic linearity

To assess linearity, we compare resilience values between those derived from empirical force–displacement data versus resilience values of a linear fit to the force–displacement data (figure 5d). For the linear fit, force and displacement amplitude were extracted via frequency domain analysis. We applied the Fourier transform to each signal. We extracted force and displacement amplitudes for each driving frequency over the frequency sweep. This technique is analogous to fitting a sinusoid to our data and has the advantage of not relying on maximum and minimum values, which can be sensitive to noise. Phase lag between force and displacement is determined by  $\phi = \tan^{-1}(E''/E')$ . Here  $E'$  is the storage modulus while  $E''$  is the loss modulus. From the phase lag,  $\phi$  and strain measurements, we generate a force–displacement ellipse. Because precompression affects  $R$ , we offset this ellipse by the force and displacement offsets measured in the thoraxes. Finally, we empirically integrate to determine  $R$ .

### 2.10.3. Statistics

To determine the frequency dependence of data, we used a linear mixed-effects model [27]. In this model, each trial was represented as a random variable. To compare data at wingbeat frequency, we used two-sided  $t$ -tests. Unless otherwise stated,  $p$ -values are

determined via two-tailed  $t$ -tests. For all manipulation experiments,  $t$ -tests are paired between the intact and manipulated thorax. All reported errors are one standard deviation. We define statistical significance as a  $p$ -value  $< 0.05$ .

## 3. Results

### 3.1. The thorax behaves like a linear, structurally damped spring

The force–displacement traces provide a preliminary assessment of the thorax's mechanical properties (figure 4a,b). The thorax required 2 N to compress under physiological conditions. This force magnitude agrees with muscle force output previously reported for *Manduca sexta* [24]. Despite its structural complexity, the thorax is well approximated as a linear material, both with and without passive musculature. Under both conditions, there is evidence of  $P_{\text{return}}$  and  $P_{\text{lost}}$  in the thorax. Because we precompressed the thoraxes to physiological conditions, the majority of the elastic energy returned occurs during the down stroke. Finally, for both the passive and removed musculature conditions, the force–displacement relationship is largely frequency-independent, with only visible differences evident between the 0.1 and 90 Hz trials. From mixed linear model regression, we found that force increased shallowly with oscillation frequency by  $1.693 \pm 0.11$  mN per Hz (figures 4a,b and 5c;  $p < 0.001$ ). In addition, resilience decreased by  $-0.052 \pm 0.002\% \text{Hz}^{-1}$  ( $p < 0.001$ ) in thoraxes with passive musculature (figure 5d). However, these trends are biologically insignificant because the magnitude of force and resilience changes from 0.1 to 90 Hz are low (9% for stiffness and 6% for resilience). The biological insignificance of this trend is especially likely because *Manduca sexta* fly within a narrow frequency range around 25 Hz [4].

To better characterize these observations, we sought a mathematical model of thorax elasticity and damping. A linear force–displacement model requires a minimum of two parameters (storage and loss). Therefore, we considered two classical two-parameter models. The Kelvin–Voigt model consists of a parallel spring and viscous damper (figure 5a, inset), as defined in equation (3.1), where  $m$  is the mass of the object,  $c$  is the damping coefficient and  $k$  is the spring stiffness. The damping force in this system is velocity dependent.

$$F(t) = m\ddot{x} + c\dot{x} + kx. \quad (3.1)$$

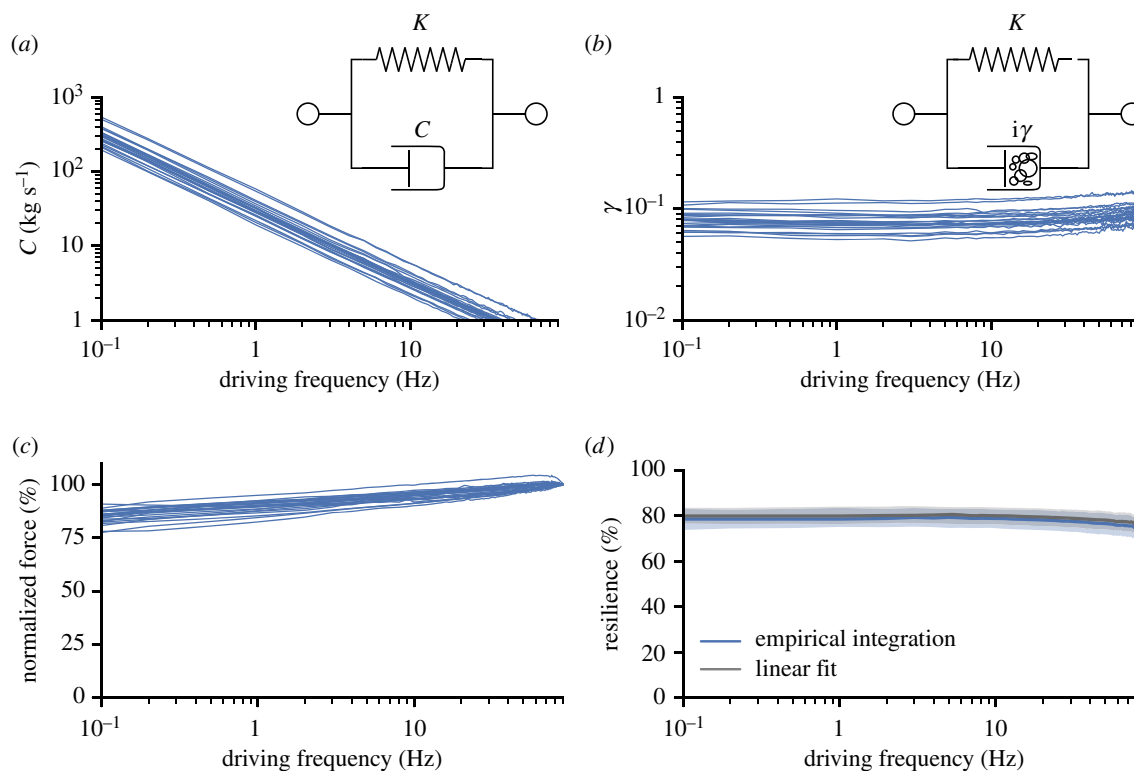


**Figure 5.** Frequency response and mechanical characterization of intact thorax with passive musculature ( $N = 24$ ). Each line denotes one individual. (a) Damping coefficient  $c$  for a Kelvin–Voigt model fit to experimental data. (b) Damping coefficient  $\gamma$  for a structural damping model fit to experimental data. (c) Normalized peak force required to deform the thorax versus frequency. For each individual, force is normalized to the peak force at 90 Hz. (d) Resilience versus calculated for experimental force–displacement data (blue) and for a linear fit (grey). Shaded area denotes one standard deviation above and below the mean. (Online version in colour.)

Next, we considered a structural damping model (figure 5b, inset and equation (3.2)) because it accurately characterized the bending of cockroach legs over a wide frequency range [28]. In this model,  $m$  is the mass of the object,  $\gamma$  is the structural damping coefficient,  $k$  is the spring stiffness and  $i = \sqrt{-1}$ . In this model, damping force is position dependent.

$$F(t) = m\ddot{x} + k(1 + i\gamma)x. \quad (3.2)$$

Both models are linear viscoelastic models but have significantly different frequency predictions. To determine the efficacy of each model, we assumed negligible mass and fit the stiffness  $k$  and loss coefficient ( $c$  or  $\gamma$ ) at each oscillation frequency.

To calculate the structural damping coefficient ( $\gamma$ ), the Kelvin–Voigt damping coefficient  $c$  and Young’s Modulus  $E$ , we first determine the storage modulus  $E'$  and the loss modulus  $E''$ . We took the Fourier transform of stress and strain at each oscillation frequency. We then divided the peak complex stress by peak complex strain to determine the complex modulus, where  $E'$  is the real portion and  $E''$  is the imaginary component. Assuming  $m$  is negligible,  $E = E'$ . Next we calculated the damping coefficients as  $\gamma = (E''/k)$  and  $c = (E''/w)$ , where  $w$  is the angular frequency of oscillation [28].

The Kelvin–Voigt damping parameter,  $c$ , changed by nearly three orders of magnitude over the driving frequency range (figure 5a). The strong frequency dependence of  $c$  indicates that the Kelvin–Voigt model is a poor representation of thorax mechanics because the thorax itself is not changing as a function of oscillation frequency. By contrast, the structural damping parameter  $\gamma$  was nearly constant over the entire driving frequency range (figure 5b). These results suggest that the thorax is best described by a structural damping model because this model has frequency-independent parameters.

There is strong agreement between resilience values from empirical force–displacement data and resilience values calculated from a linear fit of the same data (figure 5d). This suggests that deviations from linearity observed in the force–displacement data (figure 5c) do not significantly affect energetics. In summary, we conclude that the thorax behaves as a structurally damped, linear spring.

### 3.2. Passive muscle is negligible for elastic energy exchange

To assess the relative contributions of the exoskeleton and passive muscle on thorax elasticity under physiological conditions, we compared power measurements for thoraxes with passive ( $N = 24$ ) and removed ( $N = 10$ ) musculature. We found that removing the passive musculature significantly reduced the peak force to deform the thorax from  $1730 \pm 430$  mN to  $1350 \pm 250$  mN ( $p = 0.015$ ) (figure 6a). However, there was no statistical difference in resilience values between thoraxes with passive and removed musculature ( $p = 0.277$ ) (figure 6b). Although passive muscle added significant stiffness, when we divided the force–displacement plots into the respective power metrics and normalized by body mass, we found no statistically significant difference in  $P_{\text{in}}^*$  ( $p = 0.053$ ),  $P_{\text{return}}^*$  ( $p = 0.055$ ) or  $P_{\text{lost}}^*$  ( $p = 0.131$ ) (figure 6c). These results suggest that the passive thorax’s energy exchange capacity is dominated by the exoskeleton and passive muscle is negligible. However, activating muscle can engage additional elastic elements, such as cross-bridges, to increase thorax stiffness [15].

Although bulk thoracic resilience is lower than resilin [29], the thorax is stiff enough to exchange substantial energy under physiological conditions. With passive musculature, we

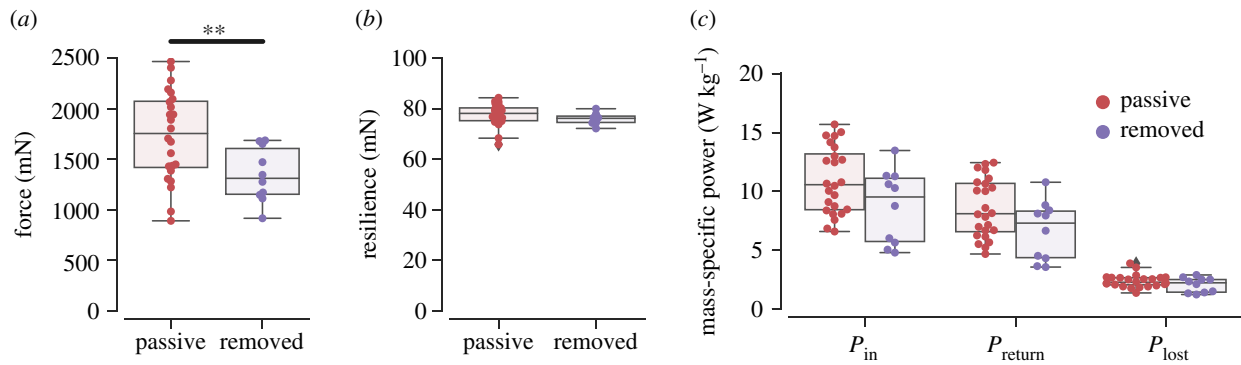


**Figure 6.** Mechanics of passive muscle are negligible. All data were taken at oscillation frequencies at 25 Hz. Boxplots denote the mean, quartiles and range of the raw data while circles are individual data points. (a) Peak force required to deform the thorax with passive ( $N=24$ ) and removed ( $N=10$ ) musculature. (b) Resilience for thoraxes with passive and removed musculature. (c) Mass-specific power measures for thoraxes with passive and removed musculature. Bar with double asterisks (\*\*) denotes statistically significant differences between conditions. (Online version in colour.)

obtained a  $P_{in}$  of  $10.9 \pm 2.8 \text{ W kg}^{-1}$ ,  $P_{return}$  of  $8.5 \pm 2.4 \text{ W kg}^{-1}$  and a  $P_{lost}$  of  $2.4 \pm 0.5 \text{ W kg}^{-1}$ . With muscle removed, we found a  $P_{in}$  of  $8.7 \pm 3.0$ ,  $P_{return}$  of  $6.7 \pm 2.4$  and  $P_{lost}$  of  $2.1 \pm 0.6 \text{ W kg}^{-1}$ .

### 3.3. Isolation of thorax regions reduces regional energy exchange performance

From visualizations of thorax strain patterns (figure 2*d*), it is evident that the wing joint and scutum move orthogonally as the thorax is stretched and compressed (figure 3*a,b*). To assess how interactions between these regions affect bulk mechanics, we performed dynamic mechanical testing on thoraxes with isolated wing joints and isolated scutums. We performed analogous experiments on a homogeneous hemisphere to ground our interpretation of these results. We used ping pong balls because they are homogeneous, structurally damped hemispheres [26]. Although ping pong balls do not possess scutums or wing hinges, we removed the analogous regions to gain intuition on how a thorax with reduced complexity might behave. In this section,  $p$ -values represent paired  $t$ -tests for thoraxes and ping pong balls pre and post manipulation.

For the ping pong ball, the isolated scutum ( $N=5$ ) had a  $P_{return}$  of only  $25.6 \pm 6.5\%$  ( $p=0.002$ ) of the intact system and a  $P_{lost}$  of  $28.5 \pm 3.5\%$  ( $p<0.001$ ). Similarly, the isolated joint ( $N=7$ ) had a  $P_{return}$  of  $27.7 \pm 5.1\%$  ( $p=0.001$ ) and  $P_{lost}$  of  $22.8 \pm 2.5\%$  ( $p=0.001$ ). Notably, strain coupling between ping pong ball regions affects both  $P_{return}$  and  $P_{lost}$  because the sum of the joint and scutum regions is less than 1 for both measures. The near monotonic decrease in  $P_{return}$  and  $P_{lost}$  led to normalized resilience values of  $99.0 \pm 2.6\%$  for the isolated scutum and  $102.7 \pm 2.0\%$  for the isolated joint. There was no statistically significant difference between the isolated scutum and the intact ping pong ball ( $p=0.474$ ), but resilience for the isolated joint significantly increased ( $p=0.015$ ). Although there is a slight increase in resilience in the ping pong ball under the isolated joint condition, these results indicate that the mechanical properties of both regions are nearly identical to that of an intact ping pong ball.

Unlike the intuition developed from the ping pong balls, isolated thorax regions see sharp decreases in spring performance. The isolated scutum ( $N=8$ ) and isolated joint ( $N=7$ ) had normalized resilience values of only  $76.6 \pm 4.1\%$  ( $p<0.001$ ) and  $82.5 \pm 3.6\%$  ( $p<0.001$ ), respectively. The

reduction in resilience is evident in the non-proportional changes in  $P_{return}$  and  $P_{lost}$ . Similar to the ping pong ball, when we isolated the scutum,  $P_{return}$  fell to  $21.9 \pm 5.5\%$  ( $p<0.001$ ) but  $P_{lost}$  only decreased to  $56.3 \pm 14.4\%$  ( $p<0.001$ ). When we isolated the joint,  $P_{return}$  for the isolated joint was  $47.5 \pm 9.1\%$  ( $p<0.001$ ) of the intact thorax. Contrary to expectations,  $P_{lost}$  remained unchanged ( $p=0.349$ ). This suggests that the majority of energy dissipation occurs in the wing joints and the addition of a scutum therefore provides free  $P_{return}$ . Similar to the ping pong balls,  $P_{return}$  benefits from mechanical coupling between regions.

### 3.4. Disruption of thoracic shape reduces energy exchange performance

Isolating thorax regions alters bulk mechanics, but it is unclear whether these effects are due to changes in strain propagation or removal of material. Therefore, we performed a series of manipulations that disrupt strain but do not remove material. In the thorax, the longitudinal cut disrupts the transverse arch, while the triple cut disrupts strain between the wing joint and scutum. Like §3.3,  $p$ -values represent paired  $t$ -tests between intact and manipulated thoraxes and ping pong balls.

For ping pong balls, disrupting the transverse arch via a longitudinal cut ( $N=7$ ) led to a  $P_{return}$  of  $81.7 \pm 3.8\%$  of the intact system ( $p=0.001$ ) and  $P_{lost}$  of  $74.2 \pm 9.8\%$  ( $p=0.013$ ). When we added two parallel cuts for the triple cut condition ( $N=7$ ),  $P_{return}$  was only  $71.9 \pm 3.6\%$  ( $p<0.001$ ) of the intact ping pong ball and  $P_{lost}$  dropped to  $68.1 \pm 10.8\%$  ( $p=0.012$ ). Similar to the region removal experiments, the nearly proportional decrease in  $P_{return}$  and  $P_{lost}$  led to normalized resilience values identical to the intact ping pong ball for both the longitudinal ( $p=0.243$ ) and triple ( $p=0.935$ ) cut conditions. This indicates that changes in strain propagation does not affect spring performance.

Similar to the ping pong balls, altering strain without removing material reduced  $P_{return}$  in thoraxes. However,  $P_{lost}$  was unchanged. For thoraxes, the longitudinal cut ( $N=8$ ) reduced  $P_{return}$  to  $88.1 \pm 7.6\%$  ( $p=0.010$ ) while  $P_{lost}$  was unaffected ( $p=0.803$ ). Similarly, the triple cut ( $N=7$ ) reduced  $P_{return}$  to  $75.1 \pm 9.9\%$  ( $p=0.002$ ) while  $P_{lost}$  remained constant ( $p=0.984$ ). Unlike the ping pong ball, changes in strain propagation did not affect  $P_{lost}$ . A constant  $P_{lost}$  but reduced  $P_{return}$  led to normalized resilience values of  $96.9 \pm$

2.3% ( $p=0.008$ ) for the longitudinal cut and  $93.1 \pm 3.4\%$  ( $p=0.002$ ) for the triple cut condition. These results indicate that strain propagation is critical for thorax mechanics because strain disruption without the removal of material significantly alters bulk mechanical properties.

## 4. Discussion

### 4.1. Frequency-dependent consequences of frequency-independent thorax mechanics

The thorax's frequency response is an important mechanical property for flight because insects may use wingbeat frequency modulation for aerodynamic force control [30,31]. In air, oscillating systems typically exhibit frequency-independent damping [26]. By contrast, interactions with fluids often introduce velocity dependencies. For example, isolated passive muscle exhibits strong frequency-dependent damping, in part due to its high water content [32–34]. Despite the presence of viscoelastic muscle, a cockroach leg exhibits frequency-independent damping [28]. Similarly in the hawkmoth, we find that the exoskeleton dominates thorax properties and exhibits frequency-independent mechanics (figure 5*b–d*).

The interactions of a frequency-independent thorax with frequency-dependent power requirements limits the range of energetically preferable wingbeat frequencies. This occurs because both  $P_{\text{inertial}}$  and  $P_{\text{aero}}$  scale cubically with wingbeat frequency [7], unlike  $P_{\text{return}}$  and  $P_{\text{lost}}$ . At high wingbeat frequencies, the thorax is unable to return sufficient elastic energy to substantially offset  $P_{\text{inertial}}$ . At low wingbeat frequencies, a large proportion of  $P_{\text{total}}$  is dissipated in the thorax ( $P_{\text{lost}}$ ). The combination of these two effects suggests a range of energetically favourable wingbeat frequencies. It is unclear whether this range corresponds to a true resonance because nonlinear aerodynamic damping, lack of accurate estimates of effective wing mass and uncertainties about transmission ratio between the muscles and wings prevents accurate estimates of resonance mechanics.

Beyond just hawkmoths, frequency-independent damping may be ubiquitous in insect joints. At many length scales, components of the insect flight apparatus exhibit frequency-independent mechanical properties. Proteins [18], composite structures [29], and now our data on *Manduca sexta* thoraxes all demonstrate frequency-independent damping. Extending beyond insect flight, both resilin and chitin are found in the spring-like structures of many arthropods [35]. Although Burrows *et al.* [36] did not perform frequency sweep experiments, they found that frog hopper insects store elastic energy in a composite structure composed predominantly of chitin and resilin. In addition, resilin is found in the joints of cockroach legs [37], which is known to exhibit frequency-independent damping [28]. The building blocks of insect joints are structurally damped, which is maintained as the systems are built up into an entire flight apparatus.

While the structural damping model accurately represents harmonic thoracic deformations, there are limitations to this model. The imaginary  $i\gamma$  term is difficult to interpret, but manifests as a phase lag between force and displacement under harmonic oscillations. For non-harmonic displacements, a signal must be decomposed into its component frequencies, which makes analysis of arbitrary signals difficult in the time

domain. Physically, frequency-independent damping can occur if a system has many stress relaxation time constants [38]. In such a system, the nearest time constant determines the system's response and can lead to the frequency-independent mechanics we observed in the thorax. Despite its limitations, the structural damping model has been used to describe a range of frequency-independent behaviour from cockroach leg bending to aerodynamic flutter [28,39] and provides a simple mathematical basis to investigate energy exchange in frequency-independent systems.

### 4.2. Thoracic exoskeleton returns the maximum amount of beneficial elastic energy

The general approach to quantify elastic energy exchange is to estimate  $P_{\text{total}}$  first assuming no elastic energy exchange, then assuming perfect elastic energy exchange. The difference between the two  $P_{\text{total}}$  estimates represents the maximum energetic benefit of spring-like structures. Using this general strategy in *Manduca sexta* but with different experimental approaches, Willmott & Ellington (blade element models), Mao & Gang (computational fluid dynamics) and Warfvinge *et al.* (particle image velocimetry) concluded that elastic energy exchange can reduce  $P_{\text{total}}$  by up to 20–35% [9–11]. To extend upon this work, Dickinson & Lighton used respirometric measurements of tethered flies combined with model-based estimates of  $P_{\text{aero}}$  and  $P_{\text{inertial}}$  [7]. They found that 11% elastic energy exchange accounted for the differences in blade element model and respirometric estimates of  $P_{\text{total}}$  in *Drosophila hydei*. However, these estimates rest on the assumption that muscle efficiency is constant. A following study showed that muscle efficiency in the closely related *Drosophila melanogaster* can vary by threefold depending on motor output [40]. In addition to modelling approaches, Weis-Fogh reported preliminary measurements of the static relationship between wing angle and torque in locusts (*Schistocera gregaria*), privet hawk moths *Sphinx ligustri* and dragonflies *Aeshna grandis* [41]. He concluded that the exoskeleton was stiff but was unable to quantify elastic energy exchange. In addition, it is unlikely that artificially backdriving the wings accurately reproduces thorax deformations seen *in vivo* because muscles are necessary to properly engage the wings into flight position [3].

We have found that the *Manduca sexta* thoracic exoskeleton returns  $8.6 \pm 2.4 \text{ W kg}^{-1}$ . Compared to computational fluid dynamics [42], robophysical [43] and kinematic estimates [10,44] of body mass specific inertial power requirements ( $P_{\text{inertial}}^*$ ), the passive thorax has the capacity to reduce  $P_{\text{inertial}}^*$  by 25–60% (figure 7). Our results agree with the previously discussed estimates of elastic energy exchange in *Manduca sexta*. For example, Willmott & Ellington estimated a maximum  $P_{\text{inertial}}^*$  reduction of  $6 \pm 3 \text{ W kg}^{-1}$ . In addition, Mao & Gang predicted that elastic structures return  $9 \text{ W kg}^{-1}$  [9]. These estimates represent the excess  $P_{\text{inertial}}$  during each halfstroke and therefore the maximum useful elastic energy return capacity. Because  $P_{\text{return}}^*$  in the thorax itself matches these estimates, energy exchange from other structures or increased thorax stiffness would not affect flight power requirements. Therefore, exoskeletal deformations alone are sufficient to reduce  $P_{\text{total}}$  to a minimum.

Adding a stiff exoskeleton has potential detriments to insect flight. Although the thorax returns significant energy, it also dissipates  $2.4 \pm 0.5 \text{ W kg}^{-1}$  that cannot be recovered (figure 7). In *Manduca sexta*, thorax elasticity leads to a net

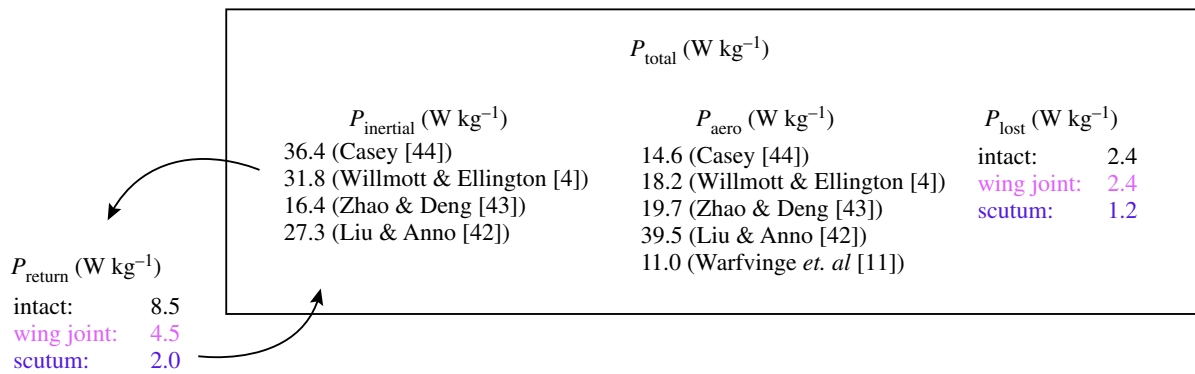


**Figure 7.** Power measurements during *Manduca sexta* flight. The total mechanical power produced by the muscles ( $P_{\text{total}}$ ) must supply  $P_{\text{inertial}}$  and  $P_{\text{aero}}$ . Here,  $P_{\text{inertial}}$  assumes zero elastic energy exchange. In addition, our results show that  $P_{\text{lost}}$  is non-negligible and substantial recycling of  $P_{\text{inertial}}$  via elastic energy exchange ( $P_{\text{return}}$ ). (Online version in colour.)

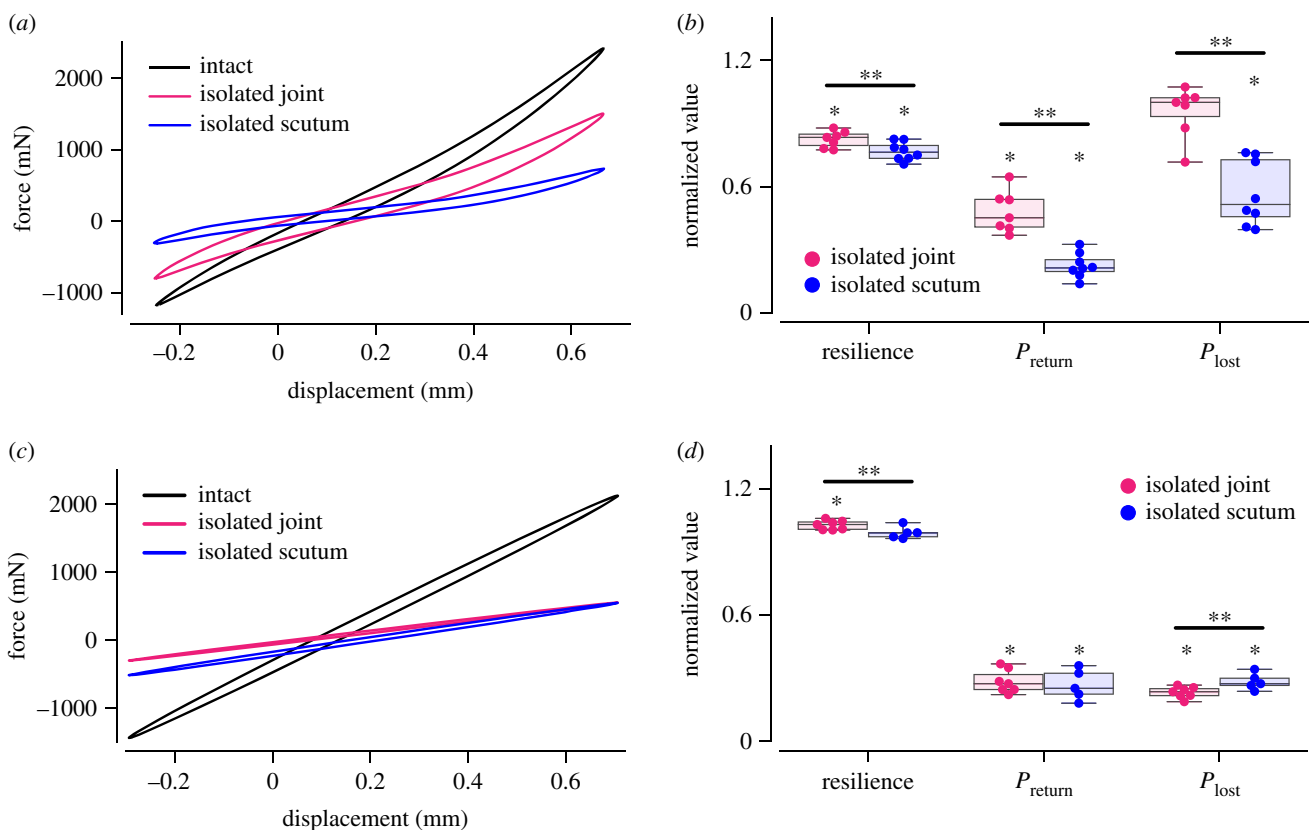


**Figure 8.** Region isolation experiments. (a) Representative force–displacement plots for an intact, isolated joint and isolated scutum thorax. At each time point, we plot the average force against the average displacement for each condition. Positive displacement denotes compression. (b) Effects of regions isolation on resilience,  $P_{\text{return}}$  and  $P_{\text{lost}}$  in thoraxes with passive musculature and isolated scutums ( $N = 8$ ) or isolated wing joints ( $N = 7$ ). All data were normalized to the paired, intact thorax and taken at an oscillation frequency of 25 Hz. Boxplots denote the mean, quartiles and range of the raw data, while circles are individual data points. Single asterisk (\*) denote a significant difference from the paired, intact thorax, whereas double asterisks (\*\*) mark differences between conditions. (c) Same as (a) but for a ping pong ball. (d) Same measures as (b) but for ping pong balls with isolated scutums ( $N = 7$ ) or isolated joints ( $N = 5$ ). (Online version in colour.)

reduction in  $P_{\text{total}}$ , but it is possible to dissipate more energy than recovered. In addition, before the wings have built up sufficient kinetic energy to deform the exoskeleton, insects must expend additional power to deform the thorax. Similarly, to rapidly accelerate the wings from a stop, *Manduca sexta* must now deform the stiff exoskeleton in addition to providing  $P_{\text{inertial}}$  and  $P_{\text{aero}}$ . To bring the wings to a sudden stop, *Manduca sexta* must rapidly dissipate stored elastic energy. However, for *Manduca sexta*, the benefits of minimizing  $P_{\text{total}}$  during sustained, steady flight may outweigh these drawbacks.

These results provide an updated perspective on the power requirements of *Manduca sexta* flight. Due to experimental

challenges in estimating  $P_{\text{inertial}}$  and  $P_{\text{aero}}$ , there is wide variability in the literature (figure 7) [10,11,42–44]. This variation has led some authors to argue that there is no benefit of elastic energy exchange because they find that  $P_{\text{aero}}$  exceeds  $P_{\text{inertial}}$  and the wing therefore has no excess kinetic energy [42,43]. However, this argument depends on the time course of  $P_{\text{inertial}}$  and  $P_{\text{aero}}$  and not the wingbeat-averaged values. In support of the elastic energy exchange hypothesis, our results show that the passive flight system has substantial energy exchange capacity. If the energy to deform the thorax does not come from excess wing kinetic energy, then *Manduca sexta* must provide this energy from muscles, which goes against an energy

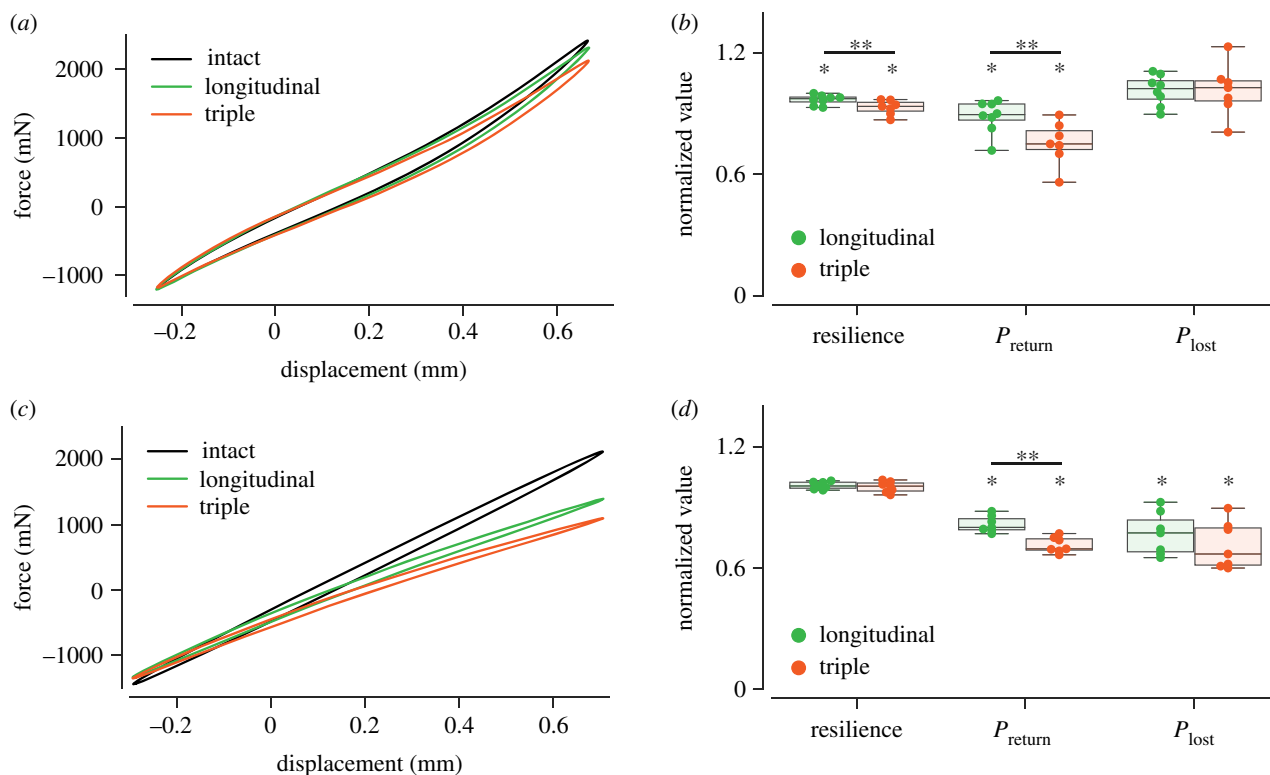


**Figure 9.** Strain disruption experiments. (a) Average force–displacement plots for an intact, longitudinal cut and triple cut thorax. At each time point, we plot the average force against the average displacement for each condition. Positive displacement denotes compression. (b) Effects of strain disruption on resilience,  $P_{\text{return}}$  and  $P_{\text{lost}}$  in thoraxes with passive musculature and a longitudinal cut ( $N = 8$ ) or triple cut ( $N = 7$ ). All data were normalized to the paired, intact thorax and taken at an oscillation frequency of 25 Hz. Boxplots denote the mean, quartiles and range of the raw data while circles are individual data points. Single asterisk (\*) denote a significant difference from the paired, intact thorax, whereas double asterisks (\*\*) mark differences between conditions. (c) Same as (a) but for ping pong balls. (d) Same measures as (b) but for ping pong balls with longitudinal cuts ( $N = 7$ ) or triple cuts ( $N = 7$ ). (Online version in colour.)

minimization strategy [45]. In addition, we find that thorax dissipation is substantial. Compared to the most recent and only direct measurement of power transferred to the surrounding air, dissipation in the thorax accounts for nearly 20% of power dissipation [11]. By dissipating substantial energy, losses in the thorax aid in wing deceleration, but reduce the maximum useful  $P_{\text{return}}$ . Therefore, under the perfect energy exchange condition,  $P_{\text{total}} = P_{\text{lost}} + P_{\text{aero}}$ .

### 4.3. Strain coupling improves energy exchange performance

Elastic energy exchange is a common theme in biology, yet animals do not possess idealized springs [2,45]. Instead, spring-like behaviour arises from physical interactions across many length scales. For instance, the composite structure of invertebrate cuticle contributes to its material properties and some authors point to material testing results as a predictor of function [18,46,47]. However, a structure's macroscopic shape can significantly alter bulk mechanics by coupling stretching and bending modes [19,48]. For invertebrates, spring-like structures are frequently materially heterogeneous and possess complex geometry, which makes it difficult to determine the factors governing spring-like behaviour [36,49,50]. Our dynamic mechanical testing experiments have identified a simple mechanical model of thorax mechanics, but it is unclear what properties of the multifunctional thorax give rise to its bulk mechanical properties.

To unravel the determinants of spring-like properties in the thoracic exoskeleton, we began by isolating two of the main functional thoracic regions and grounding our interpretation

by comparing to a structurally damped homogeneous hemisphere. We found that both ping pong balls and thoraxes exhibit shape-dependent coupling of strain between spatially separated regions. This coupling is evident in the nonlinear summation of  $P_{\text{return}}$  between regions and thorax strain visualization (figures 8*b,d* and 2*d*). As the phragma compresses the thorax (figure 1*b*), the wing joint and scutum separate (figure 2*d*; electronic supplementary material, video S1). This separation leads to tension that couples the two regions. Unlike a homogeneous hemisphere, both isolated thorax regions had lower resilience than the intact thorax. This suggests that local mechanical properties depend on global structure, perhaps due to the thorax's complex shape or material heterogeneity. To disentangle the effects of shape and material, we disrupted strain in both systems without removing material. We again observed that, unlike the homogeneous hemisphere, local resilience and therefore mechanical properties are dependent on global strain propagation (figure 9*b,d*). In addition to expected changes in stiffness, we observe that altering strain patterns in the homogeneous hemisphere can affect dissipation, but does not in the thorax. Although the thorax is well approximated with a mathematical structural damping model, the thorax's bulk mechanical properties deviate from those of a physical structurally damped model.

The discrepancy between the thorax and ping pong ball arise because functional specialization of exoskeletal regions decouples  $P_{\text{return}}$  and  $P_{\text{lost}}$ . For instance, the wing joint must withstand the high strains necessary for wing movement, whereas the scutum may be optimized for spring-like behaviour [21]. Because dissipation occurs primarily in the wing joint, the addition of scutum deformations via indirect

actuation increases  $P_{\text{return}}$  by 50% but does not increase  $P_{\text{lost}}$ . The exoskeleton's ability to return the maximum useful elastic energy may explain the general lack of tendons in insects with indirect musculature [46]. Although active muscle may recycle substantial energy, our results in tandem with previous estimates of the maximum useful elastic energy exchange suggest that spring-like behaviour in other structures would not affect  $P_{\text{total}}$  [9–11].

These results indicate that coupling between functional regions can have significant energetic consequences for biological systems. For instance, *Manduca sexta* benefits from the nonlinear summation of  $P_{\text{return}}$ . Beyond insect flight, elastic energy exchange in exoskeletal structures is a key component of power amplified behaviour [2,36,49,50]. Like other biological structures with complex geometry, the performance of spring-like structures in the thorax may be highly dependent on their integration with the global system and cannot be characterized in isolation [19,51].

## 5. Conclusion

For *Manduca sexta* and insects with indirect actuation, the power requirements directly related to wing movement ( $P_{\text{inertial}}$  and  $P_{\text{total}}$ ) as well as those associated with thorax deformations ( $P_{\text{return}}$  and  $P_{\text{lost}}$ ) are critical for flight energetics. Via dynamic mechanical testing, we establish that the thorax's mechanical properties are well approximated as a structurally damped, elastic material, which provides a useful characterization for integrated models of flapping-wing flight in insects.

## References

- Pringle JWS. 1957 *Insect flight*. Cambridge, UK: Cambridge University Press.
- Ilton M *et al.* 2018 The principles of cascading power limits in small, fast biological and engineered systems. *Science* **360**, 1082. (doi:10.1126/science.aao1082)
- Deora T, Singh AK, Sane SP. 2015 Biomechanical basis of wing and haltere coordination in flies. *Proc. Natl Acad. Sci. USA* **112**, 1481–1486. (doi:10.1073/pnas.1412279112)
- Willmott AP, Ellington CP. 1997 The mechanics of flight in the hawkmoth *Manduca sexta* I. Kinematics of hovering and forward flight. *J. Exp. Biol.* **200**, 2705–2722.
- Altshuler DL, Dickson WB, Vance JT, Roberts SP, Dickinson MH. 2005 Short-amplitude high-frequency wing strokes determine the aerodynamics of honeybee flight. *Proc. Natl Acad. Sci. USA* **102**, 18 213–18 218. (doi:10.1073/pnas.0506590102)
- Ellington CP. 1984 The aerodynamics of hovering insect flight. VI. Lift and power requirements. *Phil. Trans. R. Soc. Lond. B* **305**, 1–15. (doi:10.1098/rstb.1984.0049)
- Dickinson MH, Lighton JRB. 1995 Muscle efficiency and elastic storage in the flight motor of *Drosophila*. *Science* **268**, 87–90. (doi:10.1126/science.7701346)
- Sotavalta O. 1952 The essential factor regulating the wing-stroke frequency of insects in wing mutilation and loading experiments and in experiments at subatmospheric pressure. *Ann. Zool. Soc. Vanamo*. **15**, 1–66.
- Mao S, Gang D. 2003 Lift and power requirements of hovering insect flight. *Acta Mech. Sin.* **19**, 458–469. (doi:10.1007/BF02484580)
- Willmott AP, Ellington CP. 1997 The mechanics of flight in the hawkmoth *Manduca sexta* II. Aerodynamic consequences of kinematic and morphological variation. *J. Exp. Biol.* **200**, 2723–2745.
- Warfvinge K, KleinHeerenbrink M, Hedenström A. 2017 The power-speed relationship is U-shaped in two free-flying hawkmoths (*Manduca sexta*). *J. R. Soc. Interface* **14**, 20170372. (doi:10.1098/rsif.2017.0372)
- Zajac FE. 1989 Muscle and tendon: properties, models, scaling, and application to biomechanics and motor control. *Crit. Rev. Biomed. Eng.* **17**, 359–411.
- Dickinson M, Farman G, Frye M, Bekyarova T, Gore D, Maughan D, Irving T. 2005 Molecular dynamics of cyclically contracting insect flight muscle *in vivo*. *Nature* **433**, 330–333. (doi:10.1038/nature03230)
- Perz-Edwards RJ, Irving TC, Baumann BAJ, Gore D, Hutchinson DC, Krzic U, Porter RL, Ward AB, Reedy MK. 2011 X-ray diffraction evidence for myosin-troponin connections and tropomyosin movement during stretch activation of insect flight muscle. *Proc. Natl Acad. Sci. USA* **108**, 120–125. (doi:10.1073/pnas.1014599107)
- George NT, Irving TC, Williams CD, Daniel TL. 2013 The cross-bridge spring: can cool muscles store elastic energy? *Science* **340**, 1217–1220. (doi:10.1126/science.1229573)
- Weis-Fogh T. 1960 A rubber-like protein in insect cuticle. *J. Exp. Biol.* **37**, 889–907.
- Weis-Fogh T. 1961 Power in flapping flight. In *The cell and the organism: essays presented to Sir James Gray* (eds JA Ramsay, VB Wigglesworth), pp. 283–300. London, UK: Cambridge University Press.
- Gosline J, Lillie M, Carrington E, Guerette P, Ortlepp C, Savage K. 2002 Elastic proteins: biological roles and mechanical properties. *Phil. Trans. R. Soc. Lond. B* **357**, 121–132. (doi:10.1098/rstb.2001.1022)
- Nguyen K, Yu N, Bandi MM, Venkadesan M, Mandre S. 2017 Curvature-induced stiffening of a fish fin. *J. R. Soc. Interface* **14**, 20170247. (doi:10.1098/rsif.2017.0247)
- Tu MS, Daniel TL. 2004 Cardiac-like behavior of an insect flight muscle. *J. Exp. Biol.* **207**, 2455–2464. (doi:10.1242/jeb.01039)
- Ando N, Kanzaki R. 2016 Flexibility and control of thorax deformation during hawkmoth flight. *Biol. Lett.* **12**, 20150733. (doi:10.1098/rsbl.2015.0733)

**Data accessibility.** Raw data from dynamic mechanical testing of thoraxes and ping pong balls are available from the Dryad Digital Repository at <https://doi.org/10.5061/dryad.8gtht76jt> [52]. Strain visualization video has been uploaded as part of the electronic supplementary material.

**Authors' contributions.** J.G., N.G. and S.S. conceived and designed the study, analysed data and wrote the manuscript. J.G. ran experiments.

**Competing interests.** We declare we have no competing interest.

**Funding.** This work was supported by US National Science Foundation CAREER grant 1554790 to S.S. and U.S. National Science Foundation Physics of Living Systems SAVI student research network (GT node grant no. 1205878).

**Acknowledgements.** The authors thank James Lynch for helpful discussions and Dr Dan Goldman for access to the shaker apparatus.

22. White DC. 1983 The elasticity of relaxed insect fibrillar flight muscle. *J. Physiol.* **343**, 31–57. (doi:10.1113/jphysiol.1983.sp014880)
23. Eaton JL. 1988 Lepidopteran anatomy. *Choice Rev. Online* **26**, 26 2124–26 2124.
24. Tu MS, Daniel TL. 2004 Submaximal power output from the dorsolongitudinal flight muscles of the hawkmoth *Manduca sexta*. *J. Exp. Biol.* **207**, 4651–4662. (doi:10.1242/jeb.01321)
25. Gravish N, Franklin SV, Hu DL, Goldman DI. 2012 Entangled granular media. *Phys. Rev. Lett.* **20**, 341–354. (doi:10.1103/physrevlett.108.208001)
26. Kimball AL, Lovell DE. 1927 Internal friction in solids. *Phys. Rev.* **82**, 676–682.
27. Lindstrom MJ, Bates DM. 1988 Newton–Raphson and EM algorithms for linear models for repeated-measures data. *J. Am. Stat. Assoc.* **83**, 1014–1022. (doi:10.2307/2290128)
28. Dudek DM, Full RJ. 2006 Passive mechanical properties of legs from running insects. *J. Exp. Biol.* **209**, 1502–1515. (doi:10.1242/jeb.02146)
29. Jensen M, Weis-Fogh T. 1962 Biology and physics of locust flight. V. Strength and elasticity of locust cuticle. *Phil. Trans. R. Soc. Lond. B* **245**, 137–169. (doi:10.1098/rstb.1962.0008)
30. Sun M, Xiong Y. 2005 Dynamic flight stability of a hovering bumblebee. *J. Exp. Biol.* **208**, 447–459. (doi:10.1242/jeb.01407)
31. Dickinson MH, Lehmann FO, Chan WP. 1998 The control of mechanical power in insect flight. *Integr. Comp. Biol.* **38**, 718–728.
32. Rack PMH. 1966 The behaviour of a mammalian muscle during sinusoidal stretching. *J. Physiol.* **183**, 1–14. (doi:10.1113/jphysiol.1966.sp007848)
33. Meyer GA, McCulloch AD, Lieber RL. 2011 A nonlinear model of passive muscle viscosity. *J. Biomech. Eng.* **133**, 091007. (doi:10.1115/1.4004993)
34. Rehorn MR, Schroer AK, Blemker SS. 2014 The passive properties of muscle fibers are velocity dependent. *J. Biomech.* **47**, 687–693. (doi:10.1016/j.jbiomech.2013.11.044)
35. Andersen SO, Weis-Fogh T. 1964 Resilin. A rubberlike protein in arthropod cuticle. *Adv. Insect Physiol.* **2**, 1–65. (doi:10.1016/s0065-2806(08)60071-5)
36. Burrows M, Shaw SR, Sutton GP. 2008 Resilin and chitinous cuticle form a composite structure for energy storage in jumping by frog hopper insects. *BMC Biol.* **6**, 41. (doi:10.1186/1741-7007-6-41)
37. Neff D, Frazier SF, Quimby L, Wang RT, Zill S. 2000 Identification of resilin in the leg of cockroach, *Periplaneta americana*: confirmation by a simple method using pH dependence of UV fluorescence. *Arthropod Struct. Dev.* **29**, 75–83. (doi:10.1016/S1467-8039(00)00014-1)
38. Neubert HKP. 1963 A simple model representing internal damping in solid materials. *Aeronaut. Q.* **14**, 187–210. (doi:10.1017/S0001925900002754)
39. Fung YC. 1955 *An introduction to the theory of aeroelasticity*. Mineola, NY: Dover Publications, Inc.
40. Lehmann FO, Dickinson MH. 1997 The changes in power requirements and muscle efficiency during elevated force production in the fruit fly *Drosophila melanogaster*. *J. Exp. Biol.* **200**, 1133–1143.
41. Weis-Fogh T. 1972 Energetics of hovering flight in hummingbirds and *Drosophila*. *J. Exp. Biol.* **56**, 79–104.
42. Liu H, Aono H. 2009 Size effects on insect hovering aerodynamics: an integrated computational study. *Bioinspiration Biomimetics* **4**, 015002. (doi:10.1088/1748-3182/4/1/015002)
43. Zhao L, Deng X. 2009 Power distribution in the hovering flight of the hawk moth *Manduca sexta*. *Bioinspiration Biomimetics* **4**, 046003. (doi:10.1088/1748-3182/4/4/046003)
44. Casey TM. 1981 A comparison of mechanical and energetic estimates of flight cost for hovering sphinx moths. *J. Exp. Biol.* **91**, 117–129.
45. Dickinson MH, Farley CT, Full RJ, Koehl MAR, Kram R, Lehman S. 2000 How animals move: an integrative view. *Science* **288**, 100–106. (doi:10.1126/science.288.5463.100)
46. Dudley R. 2000 *The biomechanics of insect flight. Form function, evolution*. Princeton, NJ: Princeton University Press.
47. Hollenbeck AC, Palazotto AN. 2013 Mechanical characterization of flight mechanism in the hawkmoth *Manduca Sexta*. *Exp. Mech.* **53**, 1189–1199. (doi:10.1007/s11340-013-9726-5)
48. Yawar A, Korpas L, Lugo-Bolanos M, Mandre S, Venkadesan M. 2017 Contribution of the transverse arch to foot stiffness in humans. arXiv, arXiv:1706.04610.
49. Gronenberg W. 1996 The trap-jaw mechanism in the dacetine ants *Daceton armigerum* and *Strumigenys* sp. *J. Exp. Biol.* **199**, 2021–2033.
50. Patek SN, Nowroozi BN, Baio JE, Caldwell RL, Summers AP. 2007 Linkage mechanics and power amplification of the mantis shrimp's strike. *J. Exp. Biol.* **210**, 3677–3688. (doi:10.1242/jeb.006486)
51. Venkadesan M, Dias MA, Singh DK, Bandi MM, Mandre S. 2017 Stiffness of the human foot and evolution of the transverse arch. arXiv, arXiv:1705.10371.
52. Gau J, Gravish N, Sponberg S. 2019 Data from: Indirect actuation reduces flight power requirements in *Manduca sexta* via elastic energy exchange. Dryad Digital Repository. (doi:10.5061/dryad.8gtht76jt)